In situ reduction of gold nanoparticles in PDMS matrices and applications for large strain sensing

Donghyeon Ryu[1], Kenneth J. Loh[*1], Robert Ireland[2], Mohammad Karimzada[2], Frank Yaghmaie[2] and Andrea M. Gusman[2]

[1]*Department of Civil & Environmental Engineering, University of California, Davis, CA 95616, USA*
[2]*Northern California Nanotechnology Center (NC2), University of California, Davis, CA 95616, USA*

Abstract. Various types of strain sensors have been developed and widely used in the field for monitoring the mechanical deformation of structures. However, conventional strain sensors are not suited for measuring large strains associated with impact damage and local crack propagation. In addition, strain sensors are resistive-type transducers, which mean that the sensors require an external electrical or power source. In this study, a gold nanoparticle (GNP)-based polymer composite is proposed for large strain sensing. Fabrication of the composites relies on a novel and simple *in situ* GNP reduction technique that is performed directly within the elastomeric poly(dimethyl siloxane) (PDMS) matrix. First, the reducing and stabilizing capacities of PDMS constituents and mixtures are evaluated via visual observation, ultraviolet-visible (UV-Vis) spectroscopy, and transmission electron microscopy. The large strain sensing capacity of the GNP-PDMS thin film is then validated by correlating changes in thin film optical properties (e.g., maximum UV-Vis light absorption) with applied tensile strains. Also, the composite's strain sensing performance (e.g., sensitivity and sensing range) is also characterized with respect to gold chloride concentrations within the PDMS mixture.

Keywords: Beer-Lambert law; gold nanoparticles; nanocomposites; PDMS; strain sensing; thin film.

1. Introduction

Buildings, bridges, wind turbines, aircrafts, and naval vessels, among other types of structural systems, are subjected to a wide variety of loads throughout their service lifetimes. These loads can be due to expected operating conditions (e.g., dead and live loads), natural catastrophes (e.g., earthquakes and hurricanes), long-term environmental corrosion, and/or unexpected severe incidents (e.g., blast and impact). Regardless of whether these applied loads have been considered during design or not, damage formation is highly probable and can propagate to cause catastrophic structural failure if damage is not detected in a timely fashion. A stark example of damage-induced structural failure is the 1988 incident when the front section of an Aloha Airlines plane ripped apart in-flight due to stress-corrosion cracks that have propagated from the fuselage lap joints (Hendricks 1991). In spite of improved structural design, more stringent inspection, updated maintenance programs, the use of high-performance materials, and more than two decades of research and development, structural damage and failure still pose a significant threat to public safety, socioeconomic

*Corresponding Author, Professor, E-mail: kjloh@ucdavis.edu

prosperity, and structural owners and stakeholders. In fact and just recently in April of 2011, a 1.5 m (5 ft) hole on the front section of a Southwest Airlines aircraft tore open in-flight, potentially as a result of fatigue cracks near rivet holes on the roof and fuselage (Berger and Wilson 2011). From these examples alone, it is obvious that there remains a dire need for the development of novel robust sensing technologies capable of detecting damage and performing structural health monitoring. However, it should be noted that structural damages are complex phenomena, and different types of damage are each governed by unique sets of conditions as well as the physics or chemistry as to why they occur (e.g., impact damage versus environmental corrosion are vastly different).

While various types of damage exist and occur in structural systems, the measurement of structural strains has been highly sought after both in the field and in laboratory studies. Not only can strain measurements be used for calculating stresses within structural materials, but localized high-strains can also signify structural damage due to excessive deformation, impact, fatigue cracks, stress-corrosion cracks, and composite delamination, among many others. As a result, strain is a useful structural response parameter that can be used for assessing damage severity, but the measurement of large strains (i.e., beyond the yield limit) is often required for capturing damage features such as plastic deformation, impact, and cracks. To date, metal-foil strain gages are still widely used for measuring structural strains in laboratory and field environments. While these sensors provide accurate strain readings and are easy to use, they possess low strain sensitivities (i.e., a gage factor of approximately 2), consume high power and current, and cannot measure large strains beyond 1% or 2%. As a result, a broad array of strain transducers has entered the marketplace or is currently under development, namely semiconductor-based strain sensors (Wang *et al*. 2006), fiber optic Bragg gratings (Lee 2003), and piezoresistive nanocomposites (Loh *et al*. 2009), to name a few. Despite the various advantages they have to offer, most of them are incapable of measuring large strains.

The enhancement of the dynamic sensing range of prototype strain transducers has been investigated by incorporating flexible polymer matrices during strain sensor fabrication. For example, many different types of polymeric materials have been adopted for fabricating flexible and large strain sensors, including polystyrene (Zhou *et al*. 2008), poly(dimethyl siloxane) (PDMS) (Fudouzi and Sawada 2006), polypyrrole (Li *et al*. 2005), polyimide (Matsuzaki and Todoroki 2007), polyisoprene (Knite *et al*. 2004), Evoprene (Cochrane *et al*. 2007), and Elastosil (Martinez *et al*. 2010). In general, these flexible polymeric strain sensors have been developed so that they can be used for different applications that require the sensor to conform to complex structural shapes. For example, (Matsuzaki and Todoroki 2007) has used a flexible polyimide substrate and an ultra-flexible epoxy resin for fabricating capacitive strain sensors for tire strain monitoring. These strain sensors need to be flexible enough so that they can be freely stretched while also changing their shape along with tire deformations. On the other hand, nanomaterials have also been combined with flexible polymers in attempts for measuring large strains. In particular, a polyisoprene-carbon black nanocomposite suggested by (Knite *et al*. 2004) exhibit piezoresistivity and can measure up to 40% tensile strains. However, as with most of the strain sensors that exist in the market today, these devices still suffer from large current draw (i.e., they have low electrical resistances similar to 120 Ω metal-foil strain gages) and ultimately depend on a constant external power source for continued operations.

As a result, various research groups have been exploring the use of metallic nanoparticles (NPs) for developing optically queried strain sensors. The advantage over the more traditional piezoresistive-type strain sensors is that they can now be interrogated by light, as opposed to relying on electrical power while reducing the amount of associated circuitry required for power delivery and data

acquisition. In fact, significant numerical, theoretical, and experimental studies have been undertaken for demonstrating the applicability of metallic NPs for optically queried strain sensing. Among them, (Qian and Park 2010a) has conducted a numerical study based on Mie theory and has shown that the optical properties of gold nanoparticles (GNPs) (e.g., absorption/scattering maxima and peak shift in the plasmon resonance wavelength) change with applied tensile and compressive strains. They have also theoretically shown that tensile strain enhances spherical silver NPs' surface enhanced Raman scattering as well their far-field optical properties due to free electron dielectric function changes (Qian and Park 2010b). (Siffalovic *et al.* 2010) has fabricated a self-assembled iron oxide NP monolayer on a Mylar membrane and has experimentally shown using small-angle x-ray scattering that the average distance between the NPs changes linearly in tandem with applied tensile strains (up to 11%). However, the experimental hardware required for sensor interrogation makes these devices impractical for field applications and structural health monitoring. Therefore, other means for sensor interrogation are required, namely by measuring light absorption. For example, (Correa-Duarte *et al.* 2007) has shown that the light absorbed by silica-coated GNPs on PDMS films changes linearly when strain is applied in the range from -2% to 3%. While strain sensing has been validated, the silica-coated GNPs are deposited onto PDMS film surfaces; they are exposed on the surface and can be sensitive to the external environment. Furthermore, the strain sensing range is quite low and is not applicable for measuring large strains due to impact damage or cracks.

In this study, a simple *in situ* gold nanoparticle reduction technique is proposed for embedding GNPs in PDMS matrices, and the nanocomposite is proposed for use as an optically queried large strain sensor. First, the new *in situ* GNP reduction technique can greatly simplify the current state-of-art of embedding NPs in materials, because GNPs can be reduced by PDMS without the addition of any foreign reducing, transferring, dispersing, and stabilizing agents. This is in contrast to other more common GNP reduction and stabilization techniques that use other agents such as thiols (Kumar *et al.* 2007) and sodium citrate (Polte *et al.* 2010). Although (Goyal *et al.* 2009) has already suggested an *in situ* GNP synthesis method in PDMS matrices, the synthesis procedure still relies on methanol and methylene chloride for transferring gold chloride into PDMS. Upon validating the ability to perform *in situ* GNP reduction in PDMS, the specific reduction capability of PDMS constituents and its mixture are characterized via visual observation, ultraviolet-visible (UV-Vis) spectroscopy, and transmission electron microscopy (TEM). From the results of the aforementioned study, the optimal parameters for *in situ* reduction of GNPs in PDMS are identified. Then, five different sets of PDMS/GNP thin films are fabricated for the large strain sensing validation tests. In particular, the initial gold salt and final GNP concentration within the PDMS matrix is varied from 0.01 *wt*.% to 0.09 *wt*.% in 0.02 *wt*.% increments. Specimens from each set of PDMS/GNP films are subjected to uniaxial tension tests, and the objective is to identify the optimal GNP concentration for maximizing strain sensitivity and strain sensing dynamic range. Finally, the results and the mechanism that enables strain sensing are also explained using the Beer-Lambert law.

2. Experimental details

2.1 Materials

The *in situ* reduction of gold nanoparticles in PDMS is conducted using pellet-type gold (III) chloride trihydrate (namely gold salt or $HAuCl_4 \cdot 3H_2O$, 99.9% purity, and is obtained from Sigma-

Aldrich) and crushed using a glass rod before use. For the polymeric matrix, the *Sylgard* 184 PDMS silicone elastomer kit is purchased from Dow Corning. It should be noted that the PDMS kit consists of a base and a curing agent and is referred to as PDMS Part I and Part II, respectively. Lastly, other additional solvents, chemicals, reagents, and laboratory supplies are acquired from Fisher Scientific and are used as received.

2.2 GNP reduction and stabilization using PDMS

PDMS and gold salt mixtures are prepared to investigate the ability of individual PDMS constituents and their mixtures for reducing and stabilizing gold nanoparticles. Two metrics are used for evaluating and characterizing the mixtures. First, optical photographs and visual observations are employed for describing the color of the mixtures. A ruby red color suggests the presence of GNPs within the PDMS-based mixtures (Faraday 1857). Second, UV-Vis absorption spectroscopy provides quantitative data and can confirm the presence, relative size, and growth of GNPs within PDMS constituents and the PDMS matrix.

A total of six unique sample sets are fabricated according to Table 1, and it can be seen that they can be categorized into two groups, namely three control sample sets based on different PDMS constituents and three similar sets with the addition of gold salt. Each sample is prepared by pouring the appropriate PDMS constituents into a small beaker (Table 1). For samples based on PDMS mixtures, Parts I and II are mixed together at a 10:1.4 weight ratio, respectively. Once the different parts have been poured into the small beaker, the samples are stirred for 2 min for obtaining a homogeneous mixture and are then allowed to sit for 1 min as Parts I and II react and begin to crosslink. Then, 8 g of each of the PDMS constituents and mixtures are poured into three sets of 20 mL glass scintillation vials to form the control samples (Table 1).

On the other hand, preparation of the gold-based samples shown in Table 1 begins by carefully measuring 30 mg of gold salt into 20 mL glass scintillation vials, followed by crushing with a glass rod to form a fine powder. Then, 8 g of the previously prepared PDMS parts and mixtures are poured into the vials containing gold to form 0.374 *wt*.% PDMS-gold salt mixtures. Finally, all six sample sets are subjected to bath sonication (135 W, 42 kHz) at 60ºC for 90 min. Physical changes of the samples are monitored during sonication and throughout storage at room temperature for a period of 30 days.

For UV-Vis spectroscopic analysis, the mixtures, namely Part I/gold and Part II/gold of Table 1, are poured into methacrylate semi-micro disposable cuvettes (light path: 10 mm; capacity: 1.5 mL; Fisher Scientific). A Cary 100 UV-Vis spectrophotometer is employed for conducting absorption spectroscopy in the range from 300 nm to 900 nm at room temperature (25ºC). UV-Vis spectra are obtained immediately after mixture sonication and after storing them at room temperature for 1, 2, 4, and 30 days for evaluating the stability of GNPs via peak wavelength shifts and light absorption.

Table 1 Six unique PDMS and PDMS/GNP sample sets fabricated for characterization

Control		Control + gold salt	
Mixture	Weight [g]	Mixture	Weight [g]
Part I	8	Part I/GNP	8.03
Part II	8	Part II/GNP	8.03
Part I/II	8	Part I/II/GNP	8.03

2.3 TEM characterization of PDMS/GNP composites

Transmission electron microscopy of PDMS-gold salt mixtures is conducted for evaluating the size and morphology of reduced gold captured in PDMS matrices. Similar to Section 2.2, 0.374 *wt*.% PDMS-gold salt mixtures are prepared. However, since TEM requires very thin sample geometries, the solution preparation procedure outlined in Section 2.2 needs to be modified. Here, the PDMS Part I/II/gold salt mixture is bath sonicated in ice water for 30 min to prevent rapid PDMS polymerization due to thermal energy induced by hydrochloric acid (HCl) generation. In contrast, Part I/gold salt and Part II/gold salt mixtures are heat-sonicated at 60°C for 90 min following a similar procedure described in Section 2.2. Upon homogenization of gold salt in PDMS, toluene (anhydrous, 99.8%) is added to each mixture at a 1:1 toluene-to-PDMS mix ratio for dilution (with the exception of the Part II/GNP mixture). The solutions are again subjected to 10 min of bath sonication at room temperature for uniformly dispersing gold salt.

Then, to prepare the TEM specimens for imaging, copper grids (200 mesh copper grids with Lacey Formvar/Carbon support film from Ted Pella) are dipped into the as-prepared PDMS-gold salt mixtures, followed by absorbing excessive mixtures using filter paper, air-drying for 5 min, and then oven-drying at 60°C for 10 min. In order to further remove any abundant mixtures that have been deposited onto the copper grids (i.e., so as to obtain clear TEM images), the gold-PDMS-coated copper grids are repeatedly washed by dipping them in toluene for several times and then air drying the specimens. Visualization of GNPs within the PDMS matrix is achieved using a Philips CM-12 TEM operating at 100 kV accelerating voltage. As will be explained in Section 3.2, since gold nanoparticles are present within the polymeric matrix, the samples will be referred to as PDMS/GNP.

2.4 PDMS/GNP thin film fabrication

PDMS/GNP thin films approximately 1 mm thick are fabricated using spin coating and will be used for the strain sensing characterization tests that will be described in Section 2.5. The specimen fabrication procedure starts by preparing PDMS/GNP solutions following the mixture procedure described in Section 2.2. Here, five different batches of PDMS/GNP solutions are prepared for fabricating PDMS/GNP thin films with five different gold salt concentrations ranging from 0.01 *wt*.% to 0.09 *wt*.% in 0.02 *wt*.% increments. Specimen preparation begins by mixing PDMS Parts I and II using a 10:1.4 weight ratio, followed by vigorously stirring the mixture with a glass rod for 1 min. Upon stirring, each of the five PDMS mixtures is poured into 20 mL glass scintillation vials and immediately stirred again for 30 s with a glass stir rod. Third, the five different sets of the PDMS/GNP mixtures are degassed simultaneously for 10 min in a dessicator. The degassing process is necessary for making the PDMS/GNP thin film more uniform by eliminating entrapped air bubbles within the PDMS matrices after vigorous stirring. The five PDMS/GNP mixtures are also homogenized by subjecting them to 30 min of bath sonication in ice water to prevent them from polymerizing from the heat of reaction. Lastly, the homogenized solutions are degassed again for 5 min in a dessicator.

Using the five different PDMS/GNP mixtures, each with a different gold salt concentration, five sets of PDMS/GNP thin films are spin coated on 15 cm (6 in) silicon wafers as illustrated in Fig. 1. First, each mixture is dosed onto the wafer and is spread at 250 rpm until the mixture reaches the wafer's edge. Next, the PDMS/GNP spread is left on the wafer for 4 h to allow it to equilibrate and spread to form a uniformly thick layer before the film and wafer is transferred into a vacuum oven.

(a) PDMS/Gold Salt Mixture

(b) PDMS/GNP Dispersion

(c) PDMS/GNP Thin Film Fabrication
: Spin Coating and Oven Curing

(d) PDMS/GNP Thin Film
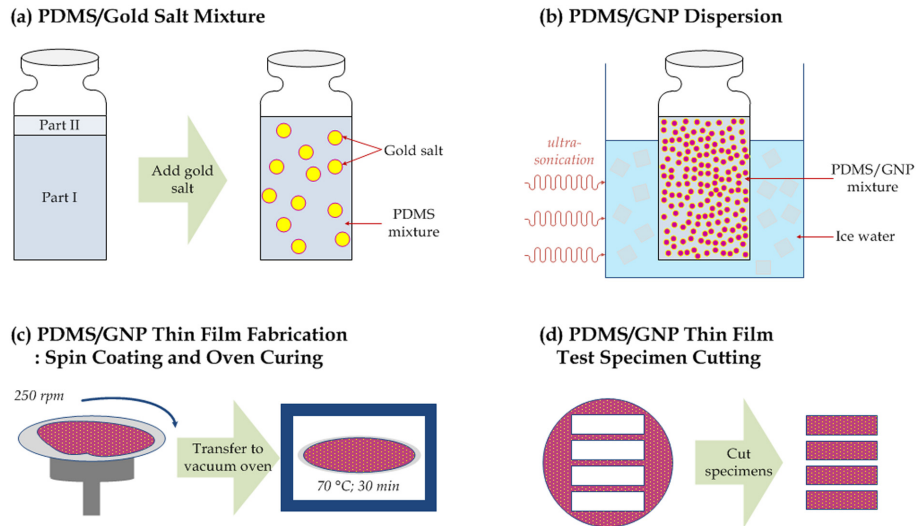**Test Specimen Cutting**

Fig. 1 A schematic illustrating the fabrication of GNP-PDMS thin films using spin coating

Table 2 Sample numbers of PDMS/GNP thin film specimens fabricated for strain sensing validation

Gold conc. [*wt.%*]	0.01	0.03	0.05	0.07	0.09
	#1	#4	#7	#11	#14
	#2	#5	#8	#12	#15
Sample number	#3	#6	#9	#13	#16
			#10		#17

Curing the spread solution for 30 min at 70°C results in highly uniform and homogeneous PDMS/ GNP thin films. Three or four strain sensing test specimens are cut and extracted from each of the five films on the silicon wafer, where each specimen is approximately 2.5 mm wide, 7.5 mm long, and 1 mm thick. Finally, a total of 17 PDMS/GNP thin film specimens are prepared for strain sensing testing and characterization (Section 2.5). The fabricated PDMS/GNP thin films are shown in Table 2.

2.5 Large strain sensing validation

Strain sensing validation of each of the 17 PDMS/GNP thin films is conducted by mounting thin film specimens in a customized tensile strain device as shown in Fig. 2. The device is fabricated such that it will fit within a UV-Vis spectrophotometer so that it can measure the film's light absorption spectrum corresponding to different increments of applied tensile strains. In this case, the spectrophotometer measures a sample's absorbance using transmitted light. At each step of applied strain, the spectrophotometer is commanded to measure the film's UV-Vis spectra in the range of 300 nm to 900 nm light wavelengths. It should be noted that GNPs absorb light at around 530 nm, whereas the PDMS matrices barely contribute to total light absorption.

In this study, the strain testing device is mounted in a Cary 100 UV-Vis spectrophotometer, and the PDMS/GNP thin film is deformed by stretching it at ~1.2 mm increments. Controlled deformation is
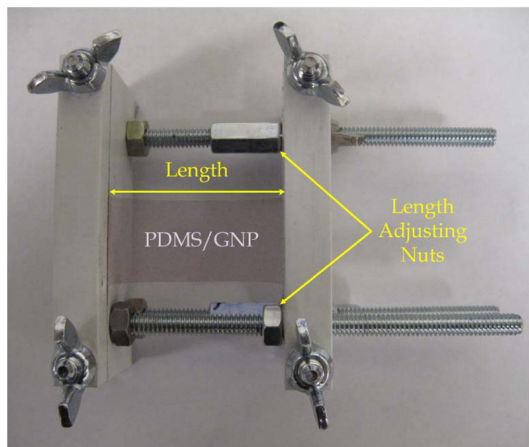
Fig. 2 A PDMS/GNP thin film is mounted in a customized tensile strain device that also fits in the Cary 100
     UV-Vis spectrophotometer used for strain sensing tests

applied in a step-wise fashion by turning the strain device's length adjusting nuts as shown in Fig. 2. While the films are deformed by approximately 1.2 mm increments, the precise length of the film is measured using a Neiko digital caliper (with 5 μm resolution) for calculating the precise applied tensile strain based on Eq. (1).

$$\varepsilon_L = \frac{\Delta L}{L_0} \qquad (1)$$

where, ε_L is strain, ΔL is the change of length of the film, and L_0 is the initial gage length or the unsupported length of the film between the two grips. Also, the PDMS/GNP thin film thickness is measured using a Mitutoyo digital thickness caliper (with 1 μm resolution). Testing continues until the films are stretched to failure.

3. Results & discussion

3.1 *In situ* reduction of gold nanoparticles in PDMS

In order to demonstrate that PDMS constituents and its mixtures are capable of reducing gold ions to form GNPs, the six sample sets of Table 1 are fabricated as specified in Section 2.2. Initially, it has been confirmed that all the pristine PDMS-based samples (i.e., control sample sets of Table 1) remain transparent before and after specimen fabrication. On the other hand, the sample sets containing gold salt change their color after mixing and after heated bath sonication as shown in Fig. 3. Here, evidence of gold reduction is confirmed visually by the appearance of a ruby red color in PDMS/GNP mixtures during and/or after heated sonication.

First, when preparing the PDMS Part II/GNP sample set, the specimens immediately show ruby red clouds after initial mixing, thereby suggesting the rapid reduction of gold to form GNPs. After 90 min of heated sonication, it can be observed that the specimen possesses a uniform ruby red color with only very small agglomerates in the mixture (Fig. 3(a)). However, while the specimen is
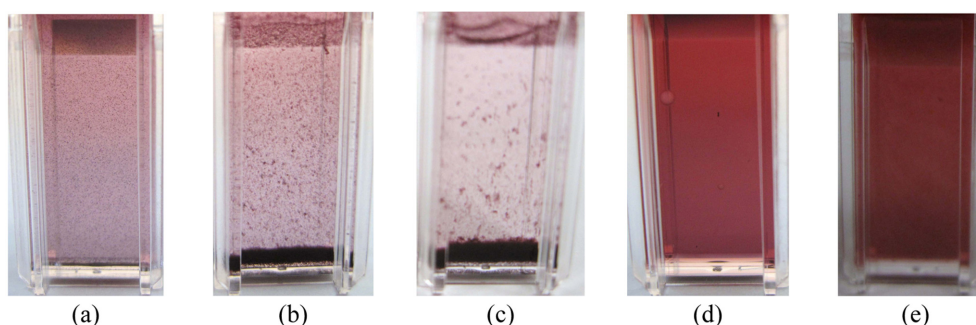
Fig. 3 Optical photographs of GNP mixtures with (a) PDMS Part II after sonication, (b) PDMS Part II after 1 day, (c) PDMS Part II after 2 days, (d) PDMS Part I after sonication and (e) PDMS Parts I/II after sonication are shown. It should be noted that the PDMS Parts I/II/GNP sample remains dispersed and in the same condition after 30 days

stored at room temperature, small precipitates begin to form. Upon further evaluation of the Part II/ GNP sample set after 1 (Fig. 3(b)) and 2 days (Fig. 3(c)), GNPs continue to agglomerate and precipitate out of PDMS Part II and then finally settling to the bottom of the vials. The continued agglomeration and precipitation of gold is due to the lack of a stabilizing structure (e.g., a crosslinked PDMS matrix) to prevent GNPs from interacting and agglomerating with one another.

In contrast to the findings presented by (Goyal *et al.* 2009), this study shows that Part I is in fact capable of reducing gold ions to form gold nanoparticles. When Part I is mixed with gold salt, the solution transitions from transparent to a light yellow color during heated sonication; it is after 60 min of heated sonication that the mixture becomes ruby red as shown in Fig. 3(d). It can be seen from Fig. 3(d) that a uniform dark ruby red specimen is obtained. The dark ruby red color confirms that PDMS Part I is capable of reducing gold. Here, the dissolved gold ions are reduced by the reaction of chloride ions with hydrogen ions present in the silicon-hydrogen (Si-H) bonds within PDMS Part I. As compared to PDMS Part II, the reduction rate of Part I is significantly slower, which is primarily due to the absence of metallic catalysts inherent to Part II. In fact, the viscous solution remains the same color and uniformity even after being stored for 30 days at room temperature. However, it should be noted that, in a separate experiment using higher concentrations (1 *wt*.%) of gold salt in Part I, some yellow gold macro-particles are precipitated because the Part I/ GNP solution does not polymerize and crosslink. Thus, while Part I is capable of reducing gold, other means are necessary to prevent GNP agglomeration and precipitation after long periods of time.

As mentioned in Section 2.2, in addition to PDMS constituents and gold salt mixtures, crosslinked PDMS Part I/II/GNP mixtures have also been prepared. Fig. 3(e) shows a picture of a solid-state Part I/II/GNP specimen. As expected, Part I/II and Part I/II/GNP mixtures polymerize after heated sonication to form a solid elastomeric matrix. For the Part I/II/GNP mixture in Fig. 3(e), GNPs are reduced as fast as the aforementioned Part II/GNP mixture, and the specimen shows a ruby red color without observable agglomerates. Again, the rapid formation of GNPs is due to the fast reduction capabilities of PDMS Part II within the mixture. More importantly, the PDMS Parts I/II/ GNP sample set remains in the same state as that shown in Fig. 3(e) over long periods of time. This result shows that, due to crosslinking of PDMS Parts I/II, GNPs are successfully captured in the elastomer's crosslinked matrix and are prevented from interacting and precipitating out of the PDMS matrix.
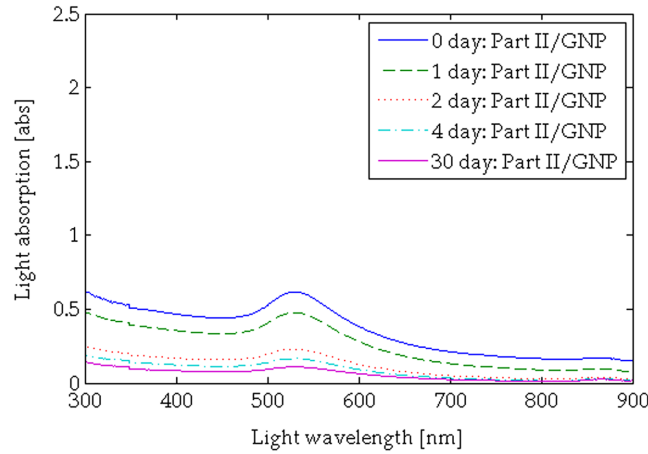
Fig. 4 UV-Vis absorption spectroscopy has been conducted on the PDMS Part II/GNP specimens immediately after sonication and over a period of up to 30 days after sample preparation. The UV-Vis spectra taken at different times show that light absorption decreases with time, thereby indicating that GNPs agglomerate and precipitate out of Part II

In addition to visual observations, UV-Vis absorption spectroscopy has also been conducted for quantifying the reduction of gold to form GNPs using PDMS as outlined in Section 2.2. First, preliminary results show that the control specimens of Table 1 exhibit negligible absorption over light wavelengths from 300 nm to 900 nm. Secondly, representative UV-Vis spectra for Part II/GNP and Part I/GNP are shown in Figs. 4 and 5, respectively. The UV-Vis spectra that have been measured over a course of 30 days are also overlaid in each of the plots as shown in Figs. 4 and 5. In general, all the UV-Vis plots show maximum absorption at approximately 530 nm, which is indicative of GNP presence in the mixtures (Zhou *et al.* 2009).

Specifically, Fig. 4 shows that the peak UV-Vis wavelength occurs at 530 nm for the Part II/GNP
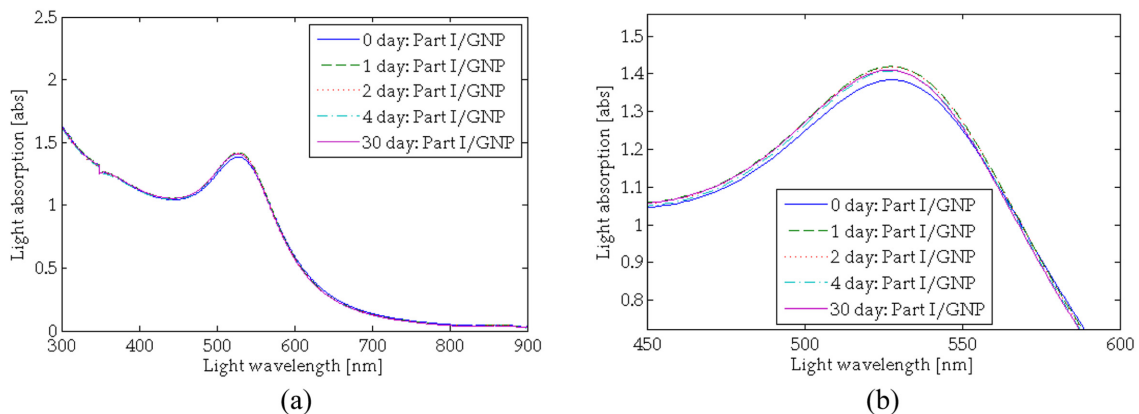

(a) (b)

Fig. 5 The UV-Vis absorption spectra for PDMS Part I/GNP mixture immediately after sonication and up to 30 days after sample preparation are shown. The UV-Vis spectra taken at different times show that the Part I/GNP mixture remain fairly stable (a) in the range from 300 nm to 900 nm and (b) from 450 nm to 600 nm. Part I reduces gold but at a very slow rate, and as a result, agglomeration occurs but also at a very slow rate

mixture, and the overall light absorption over the entire range of wavelengths decreases with increasing time. This is consistent with the conclusions drawn from previous visual observations where PDMS Part II rapidly reduces gold, but in the absence of a crosslinked matrix, GNPs will continue to reduce, agglomerate, and finally precipitate. GNP precipitation results in a diminished light absorption as can be seen in Fig. 4 since fewer GNPs remain dispersed in the mixture. In contrast, the Part I/GNP UV-Vis spectra of Fig. 5(a) show quite consistent light absorption and maximum peak wavelength throughout the 30-day measurement period. The consistent UV-Vis spectra confirm that Part I reduces gold and that agglomeration takes place at a very slow rate as have already been visually observed. On the other hand, when GNPs are reduced *in situ* within a PDMS I and II matrix, their UV-Vis response and absorption remains constant since gold nanoparticles are captured and stabilized within the crosslinked matrix.

3.2 TEM characterization of PDMS/GNP composites

As mentioned in Section 2.3, TEM has been conducted for all of the gold-based sample sets listed in Table 1. Fig. 6 shows representative TEM images of PDMS Part I/GNP, II/GNP, and I/II/GNP films prepared on a copper grid. For Part I/GNP, it has already been suggested in Section 3.1 that Part I can reduce gold, but the lack of polymerization and crosslinking allows for slow but eventual GNP agglomeration. Fig. 6(a) shows agglomerated GNPs in chain-like shapes which confirms that Part I cannot solely capture and stabilize GNPs. Nevertheless, GNPs formed by the reduction of Part I seem to have a highly uniform size distribution, thereby also suggesting that gold salt is polydispersed uniformly in Part I, and reduction takes place at a slow rate; this can also be observed from the inset of Fig. 6(a) which shows a very uniform size distribution of GNPs approximately 10 nm in diameter. In Fig. 6(b), a Part II/GNP TEM image is presented. GNPs within the Part II matrix exhibit a diverse size distribution ranging from 1 nm to 32 nm; this confirms that reduction occurs rapidly, and agglomerations also evolve quickly. Finally, Fig. 6(c) shows that GNPs within a crosslinked PDMS Part I/II structure are well spaced among one another and suggest that the crosslinked matrix is capable of stabilizing GNPs to prevent them from agglomerating and precipitating out of the bulk matrix. The size distribution of GNPs range from 7 nm to 22 nm and is much narrower than those formed when using Part II alone. From all the TEM images in Fig. 6, it can be seen that the GNPs reduced by Part I, II, and I/II are all spherical nanoparticles.
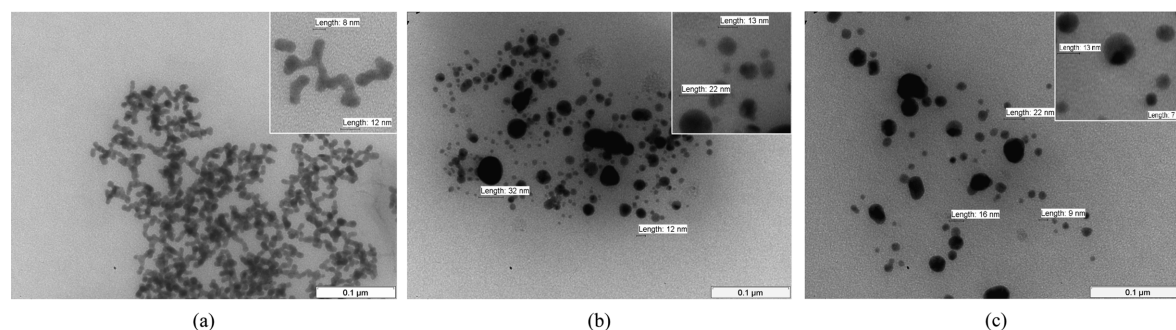

(a) (b) (c)

Fig. 6 TEM images of (a) Part I/GNP, (b) Part II/GNP and (c) Part I/II/GNP mixtures coated onto copper grids show the in situ reduction of gold salt to form gold nanoparticles

3.3 Large strain sensing validation of PDMS/GNP thin films

As described in Section 2.4 and shown in Table 2, a total of 17 strain sensing test specimens are prepared from five unique batches of PDMS/GNP mixtures. Specifically, each of the five sample sets is characterized by a distinct gold salt concentration, namely 0.01, 0.03, 0.05, 0.07, and 0.09 *wt*.%. Upon sample preparation, each film is mounted in a strain testing device, and the film's UV-Vis response is obtained at each applied strain increment as described in Section 2.5. Fig. 7(a) shows the overlay of UV-Vis spectra for the #12 PDMS/GNP thin film specimen (i.e., 0.07 *wt*.% gold salt within PDMS) over the course of the entire test after it has been stretched up to about 30% tensile strains before ultimate failure. The zoomed-in UV-Vis spectra around 530 nm show the decreasing trend of light absorption with increasing applied tensile strains (Fig. 7(b)). Thus, the proposed PDMS/GNP thin film can be used as a strain sensor if light absorption corresponding to the peak wavelength is calibrated to the level of applied strain.

In order to demonstrate that the Beer-Lambert law applies and to verify the relationship between maximum light absorption around 530 nm and applied longitudinal tensile strain, absorption is plotted as a function of thickness as shown in Fig. 8. Fig. 8 plots the results for all 17 specimens, and all the results follow the Beer-Lambert law based on two observations: (1) there exists a linear relationship between light absorption and light path length (i.e., PDMS/GNP thin film thickness), and (2) a greater slope is observed for specimens with higher GNP concentrations. It should be noted that the extinction coefficient of GNPs within all PDMS/GNP specimens are assumed to be identical because GNPs are identically reduced while following an identical preparation procedure as explained in Section 2.4. Thus, maximum light absorption can be used as strain measurement readouts based on the two aforementioned findings.

Given that light absorption is dependent on applied strain, one can also characterize the PDMS/GNP thin film's strain sensing performance. Fig. 9 plots the change in light absorption of the thin films at approximately 530 nm as a function of applied strain; only one representative result for each gold concentration sample set is plotted for clarity and comparison purposes. In addition to the raw data, linear least-squares best-fit lines are also computed and plotted in Fig. 9. It can be easily
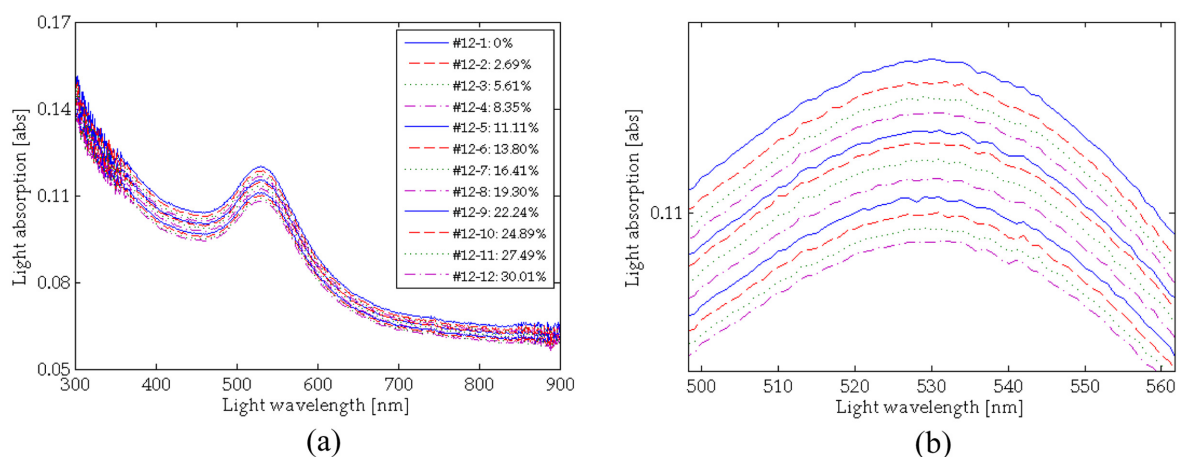

(a)   (b)

Fig. 7 The UV-Vis spectra of a PDMS/GNP thin film with 0.07 *wt*.% GNPs (sample #12) at 12 different tensile strain levels are overlaid (a) in the range from 300 nm to 900 nm and (b) from 500 nm to 560 nm. The results show that applied tensile strain decreases the overall light absorption
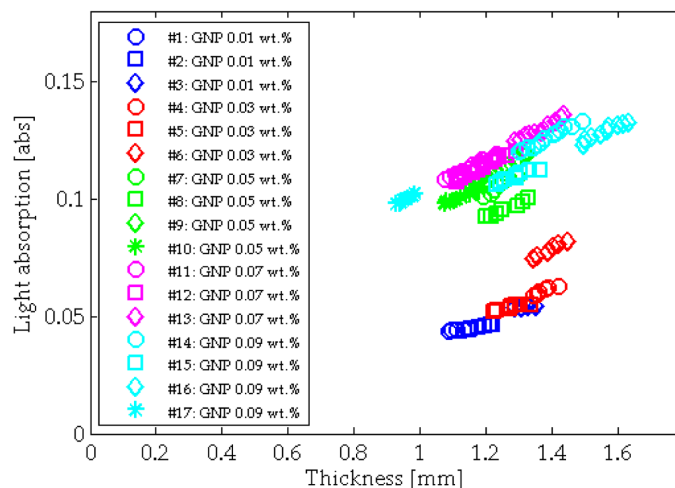
Fig. 8 The light absorption measured at 530 nm of all the 17 PDMS/GNP specimens decrease linearly in tandem with decreasing film thickness or light path length due to the application of tensile strains. The linear relationship verifies that the Beer-Lambert law is applicable for describing the relationship between light absorption and applied strains to the PDMS/GNP specimens
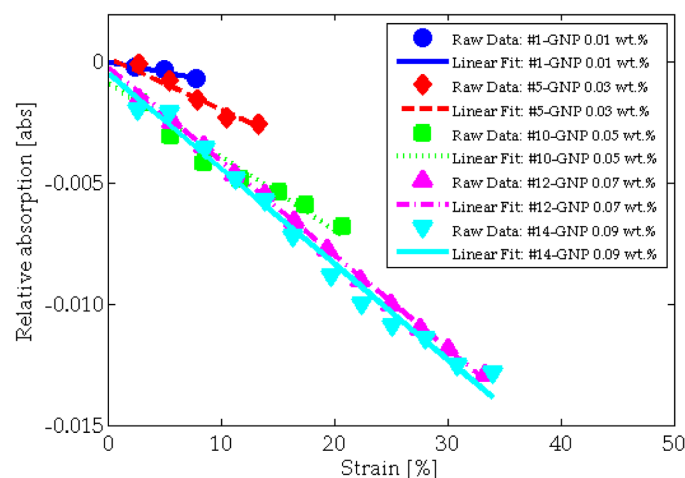

Fig. 9 The change in light absorption measured at 530 nm of representative PDMS/GNP thin films with different gold concentrations are plotted as a function of applied tensile strains. Linear least-squares best-fit lines are also overlaid along with the raw data to show that light absorption decreases linearly with increasingly applied strains

observed that specimens with higher concentrations of GNPs possess a greater slope and thus higher strain sensitivities. In addition, films with more or higher concentrations of GNPs also appear to possess larger strain sensing dynamic ranges.

In fact, Fig. 10(a) plots PDMS/GNP average strain sensitivities with respect to GNP concentrations, and Fig. 10(b) shows the relationship between strain sensing range and GNP concentrations. It can be seen from Fig. 10(a) that the average strain sensitivity is at its peak when there is approximately 0.05 *wt.*% of gold salt in the PDMS matrix. Any additional gold salt within the elastomer results in

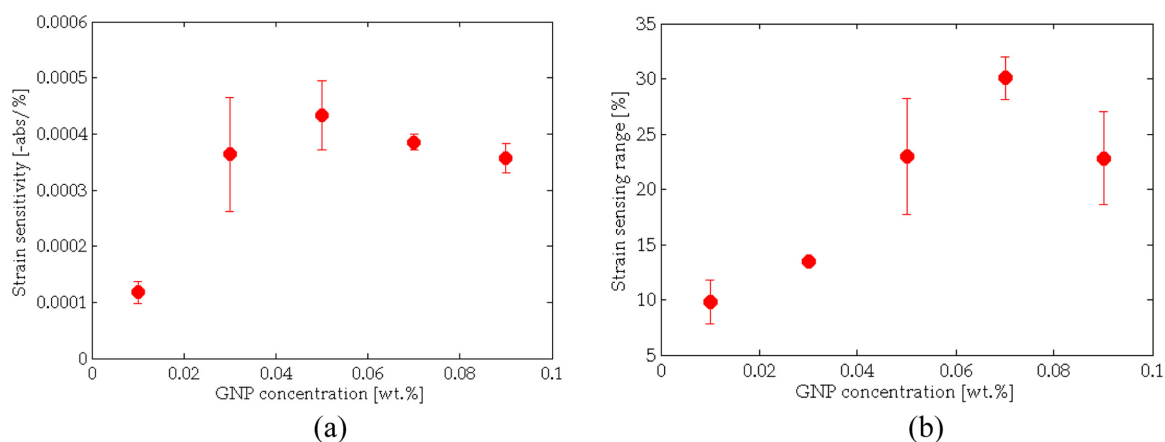(a)   (b)

Fig. 10 The strain sensing performance of PDMS/GNP thin films depend on the concentration of GNPs
embedded within the PDMS matrix. (a) The PDMS/GNP average strain sensitivities are plotted with
respect to GNP concentrations and (b) the strain sensing range is also plotted as a function of GNP
concentrations. Optimal strain sensitivity and sensing range can be achieved by using 0.07 *wt*.% gold
nanoparticles embedded within the PDMS matrix

a slight decrease in strain sensitivity. Regardless, the 0.05 *wt*.% concentration sample set has
exhibited the highest average strain sensitivity of approximately -0.00043 abs/% (Fig. 10(a)). On the
other hand, the strain sensing range of each sample set is also evaluated depending on gold salt
concentrations. In general, higher concentration specimens tend to be able to monitor and withstand
higher levels of tensile strain before they fail. For example, one of the 0.07 *wt*.% gold salt specimens
can measure tensile strains as high as 30%. The large strain sensing capacity of PDMS/GNP films is
hypothesized to be due to the highly elastic PDMS matrix, while light absorption changes are
contributed by the embedded GNPs. However, it should be mentioned that 0.09 *wt*.% specimens show
lower strain sensing ranges due to earlier fracture failure of the films. The early failure of these
films at approximately 23% strains suggests that higher GNP concentrations lower the mechanical
toughness of the PDMS/GNP thin films, because GNPs can be considered to be defects within the
elastomeric PDMS matrix. All in all, these results suggest that the optimal GNP concentration is
0.07 *wt*.% for maximizing strain sensitivity and strain sensing range.

   In addition to the experimental aspects of strain sensing validation, changes in PDMS/GNP thin
film optical properties are also investigated and characterized using the Beer-Lambert law (Eq. (2))

$$A = \varepsilon \cdot c \cdot L \tag{2}$$

where A is light absorptivity (in *abs*), ε is the extinction coefficient (in $L \cdot mol^{-1} \cdot cm^{-1}$), c is the
concentration of the compound in solution (i.e., in this case, GNPs in $mol \cdot L^{-1}$), and L is the path length
of the sample (in cm). Here, the maximum UV-Vis light absorption around 530 nm is correlated with
the path length or the thickness of PDMS/GNP thin films. Based on Beer-Lambert law and Eq. (2), it is
expected that light absorption will change in tandem with changes in the thickness of PDMS/GNP thin
films, especially since the extinction coefficient and GNP concentration remain constant.

   As have been observed experimentally, the decreasing light absorptivity of PDMS/GNP thin films
with applied tensile strain can be explained by its decrease in light path length as the film becomes

thinner due to Poisson's effect. A similar study by (Correa-Duarte *et al.* 2007) has shown that a GNP layer deposited on the surface of a PDMS thin film also exhibits a decrease in light absorption with applied tensile strains. Their results suggest that the decreasing trend of light absorption with increasing tensile strains is due to decreasing numbers of GNPs within the fixed beam area interrogated by the UV-Vis spectrophotometer. Because the layer-by-layer-assembled GNP layer is on the surface of a PDMS thin film, tensile strain causes cracks to form in the GNP layer. As more deformation is applied and the crack width increases, less GNPs are present in a given area to cause light absorption to decrease. In contrast, this study embeds GNPs within PDMS matrices. While cracking has not been observed during tensile testing, the same strain sensing mechanism exists where less gold nanoparticles are present in a given area to contribute to the total measured absorption during UV-Vis spectroscopy as the nanocomposite is being strained in tension. It should be noted that the elastomeric PDMS/GNP thin film is assumed to possess a constant Poisson's ratio. Thus, applied strain in its longitudinal direction can be directly correlated to its change in thickness to cause a measurable change in light absorption.

4. Conclusions

In conclusion, the objective of this research is to characterize the *in situ* reduction of gold nanoparticles using PDMS mixture and then validating the nanocomposite for large strain sensing applications. First, the reducing and stabilizing capabilities of PDMS constituents and their mixtures are investigated based on visual observation, UV-Vis spectroscopic analysis, and TEM imaging. As verified by many researchers, appearance of a ruby red color suggests the presence of GNPs. All of the mixtures (i.e., PDMS Part I/GNP, Part II/GNP, and Parts I/II/GNP) show a ruby red color. Among them, PDMS Part II/GNP mixture turns ruby red in the shortest amount of time, which means that Part II has the most vigorous GNP reducing capacity.

Using UV-Vis, the maximum peak absorption at around 530 nm indicates GNP presence in all of the samples. Furthermore, the stabilization capacity of Parts I and II can be evaluated by observing changes in light absorption over time. Part I has been shown to reduce gold at a much slower rate as compared to Part II based on minimal changes in light absorption over 30 days of UV-Vis measurements. TEM images also confirm that GNPs are formed when using PDMS Part I and II alone and that GNPs are also captured within a crosslinked PDMS Parts I/II/GNP matrix. Specifically, the TEM image of a Part I/II/GNP mixture indicates that GNPs are formed in the range from 7 nm to 22 nm in diameter. Therefore, gold salt can be reduced using only PDMS constituents, whereas complete stabilization can be attained using the crosslinked PDMS matrix. It should be reiterated that gold nanoparticles are reduced without adding any foreign reducing, transferring, dispersing, and stabilizing agents using the proposed *in situ* reduction technique.

For the second half of this study, tensile strain sensing validation tests have been conducted on spin coated PDMS/GNP thin films fabricated from five different PDMS/GNP mixtures with different gold salt concentrations (i.e., from 0.01 *wt.*% to 0.09 *wt.*% in 0.02 *wt.*% increments). The light absorption of the films corresponding to different levels of applied strain are measured using a UV-Vis spectrophotometer. For all of the 17 samples tested, it has been shown that light absorption decreases with increasingly applied tensile strains. The change in light absorption is due to changes in film thickness resulting from Poisson's effect as longitudinal strain is applied to stretch the films, and the results have also been verified using the Beer-Lambert law. In fact, it is verified that light

absorption of the PDMS/GNP thin films exhibit a linear relationship with film thickness and thus obeys the Beer-Lambert law.

When comparing the absorption response as a function of applied strain for the PDMS/GNP specimens with different concentrations of GNPs, it has been found that an optimal gold nanoparticle concentration exhibits for maximizing strain sensitivity and strain sensing dynamic range. In particular, PDMS/GNP specimens with 0.05 *wt.*% GNP concentrations possess maximum strain sensitivities of approximately -0.00043 abs/%. Greater GNP concentrations slightly decrease strain sensitivity. On the other hand, PDMS/GNP specimens with 0.07 *wt.*% exhibit the widest strain sensing range and can be stretched to more than 30% of its original length. Again, more GNPs reduce its strain sensing range because GNPs can serve as defects within the film and cause fracture failure. All in all, the optimal gold nanoparticle concentration for strain sensing is 0.07 *wt.*% since this simultaneously maximizes strain sensitivity and sensing range. In future work, the sensitivity of PDMS/GNP specimens to ambient and harsh external environments will be characterized. Examples include assessing its temperature and humidity sensitivities so as to determine its suitability for structural health monitoring of different types of structural systems. The possibility of PDMS/GNP composites for fiber optic-based sensing will also be studied.

Acknowledgements

References

Berger, J. and Wilson, D. (2011), *Hole in Southwest Jet Attributed to Cracks*, The New York Times.
Cochrane, C., Koncar, V., Lewandowski, M. and Dufour, C. (2007), "Design and development of a flexible strain sensor for textile structures based on a conductive polymer composite", *Sensors*, **7**(4), 473-492.
Correa-Duarte, M.A., Salgueirino Maceira, V., Rinaldi, A., Sieradzki, K., Giersig, M. and Liz-Marzan, L.M. (2007), "Optical strain detectors based on gold/elastomer nanoparticulated films", *Gold Bull.*, **40**(1), 6-14.
Faraday, M. (1857), "The bakerian lecture: experimental relations of gold (and other metals) to light", *Philos. T. R. Soc. L.*, **147**, 145-181.
Fudouzi, H. and Sawada, T. (2006), "Photonic rubber sheets with tunable color by elastic deformation", *Langmuir*, **22**(3), 1365-1368.
Goyal, A., Kumar, A., Patra, P.K., Mahendra, S., Tabatabaei, S., Alvarez, P.J.J., John, G. and Ajayan, P.M. (2009), "In situ synthesis of metal nanoparticle embedded free standing multifunctional PDMS films", *Macromol. Rapid Comm.*, **30**(13), 1116-1122.
Hendricks, W.R. (1991), *The Aloha Airlines accident - A new era for aging aircraft,* (Eds. S.N. Atluri, S.G. Sampath and P. Tong) , Structural integrity of aging airplanes, Berlin and New York: Springer-Verlag.
Knite, M., Teteris, V., Kiploka, A. and Kaupuzs, J. (2004), "Polyisoprene-carbon black nanocomposites as tensile strain and pressure sensor materials", *Sensor Actuat A-Phys.*, **110**(1-3), 142-149.
Kumar, P.S., Pal, S.K., Kumar, S. and Lakshminarayanan, V. (2007), "Dispersion of thiol stabilized gold nanoparticles in lyotropic liquid crystalline systems", *Langmuir*, **23**(6), 3445-3449.
Lee, B. (2003), "Review of the present status of optical fiber sensors", *Opt. Fiber Technol.*, **9**(2), 57-79.

Li, Y., Cheng, X.Y., Leung, M.Y., Tsang, J., Tao, X.M. and Yuen, M.C.W. (2005), "A flexible strain sensor from polypyrrole-coated fabrics", *Synthetic Met.*, **155**(1), 89-94.

Loh, K.J., Hou, T.C., Lynch, J.P. and Kotov, N.A. (2009), "Carbon nanotube sensing skins for spatial strain and impact damage identification", *J. Nondestruct. Eval.*, **28**(1), 9-25.

Martinez, F., Obieta, G., Uribe, I., Sikora, T. and Ochoteco, E. (2010), "Polymer-based self-standing flexible strain sensor", *Sensors*, **2010**.

Matsuzaki, R. and Todoroki, A. (2007), "Wireless flexible capacitive sensor based on ultra-flexible epoxy resin for strain measurement of automobile tires", *Sensor Actuat A-Phys.*, **140**(1), 32-42.

Polte, J., Ahner, T.T., Delissen, F., Sokolov, S., Emmerling, F., Thunemann, A.F. and Kraehnert, R. (2010), "Mechanism of gold nanoparticle formation in the classical citrate synthesis method derived from coupled In Situ XANES and SAXS evaluation", *J. Am. Chem. Soc.*, **132**(4), 1296-1301.

Qian, X. and Park, H.S. (2010a), "The influence of mechanical strain on the optical properties of spherical gold nanoparticles", *J. Mech. Phys. Solids*, **58**(3), 330-345.

Qian, X. and Park, H.S. (2010b), "Strain effects on the SERS enhancements for spherical silver nanoparticles", *Nanotechnology*, **21**(365704), 1-8.

Siffalovic, P., Chitu, L., Vegso, K., Majkova, E., Jergel, M., Weis, M., Luby, S., Capek, I., Keckes, J., Maier, G. A., Satka, A., Perlich, J. and Roth, S.V. (2010), "Towards strain gauges based on a self-assembled nanoparticle monolayer—SAXS study", *Nanotechnology*, **21**(385702), 1-5.

Wang, X., Zhou, J., Song, J., Liu, J., Xu, N. and Wang, Z.L. (2006), "Piezoelectric field effect transistor and nanoforce sensor based on a single ZnO nanowire", *Nano Lett.*, **6**(12), 2768-2772.

Zhou, J., Gu, Y., Fei, P., Mai, W., Gao, Y., Yang, R., Bao, G. and Wang, Z.L. (2008), "Flexible piezotronic strain sensor", *Nano Lett.*, **8**(9), 3035-3040.

Zhou, M., Wang, B., Rozynek, Z., Xie, Z., Fossum, J.O., Yu, X. and Raaen, S. (2009), "Minute synthesis of extremely stable gold nanoparticles", *Nanotechnology*, **20**(505606), 1-10.

BS